Nuclear Data for Science and Technology (1988 MITO), 407- 410, Copyright © 1988 JAERI.

FISSION FRAGMENT DISTRIBUTIONS IN RESOLVED RESONANCES OF $^{235}U(n,f)$

Franz-Joseph Hambsch*, Hans-Hermann J. Knitter, Carl Budtz-Jørgensen**

Commission of the European Communities,
Joint Research Centre - Geel-Establishment,
Central Bureau for Nuclear Measurements, 2440 Geel, Belgium.

Jürgen P. Theobald

Physikalisches Institut, Technische Hochschule
D-6100 Darmstadt, W-Germany

Abstract: Fission fragment energies and emission angles with respect to the incident neutron beam were measured for $^{235}U(n,f)$ using a twin Frisch-gridded ionization chamber. The neutron energy range from 0.006 eV to 0.5 MeV was covered in a time-of-flight experiment at the Geel Electron Linear Accelerator (GELINA). Fission fragment mass-, and total kinetic energy distributions were evaluated for thermal neutrons, for resolved resonances below 40 eV, and in certain energy bins at higher neutron energy. Fluctuations in the average total kinetic energy <TKE> with respect to the thermal value of up to ~450 keV are observed for resonances below 40 eV. The variations of <TKE> from resonance to resonance can be related to changes in the population of the three fission exit channels. Also the symmetric fission yields or valley to peak ratios of the mass distributions fluctuate from resonance to resonance up to a factor 2. Both fluctuations are not correlated with the resonance spin of the compound nucleus. An explanation for the fluctuations is proposed.

($^{235}U(n,f)$, resolved resonances, fission fragment mass-and total kinetic energy distributions, multi-exit channel model.)

1. Introduction

Fission is described by a continuous sequence of nuclear surface shapes starting from a more or less spherical shape which elongates, necks-in, and splits into two more or less deformed fragment shapes. This development of the geometrical nuclear configuration is accompanied by considerable changes of the nuclear potential energy, which in general is displayed by potential landscapes i.e. mappings of the shell and pairing corrected liquid drop potential as function of deformation coordinates. The sequence of shapes of the fissioning nucleus described by elongation-, neck-, and mass asymmetry-parameters is characterized by a path in the potential landscape. The motion along this path is affected by inertia and viscosity of the fissioning nuclear matter.

It is a longstanding question, at which point of the fission path the mass and energy distributions of the fission fragments are determined. There exist several versions of "saddle point models" and "scission point models" which put this crucial point closer to or on the (second) saddle or let it coincide with the scission point, where stability properties of the fragments become active. However none of the previous theories and fission models give a satisfactory description of the experimentally observed variances of the fragment total kinetic energy-, and mass distributions as stated by Oganessian and Lazarev /1/.

Recently a more elaborate model has been proposed by U. Brosa, S. Grossmann and A. Müller /2,3/. This model introduces additional decision elements for fragment mass and energy distributions, i.e. "bifurcation points", where the fission path splits into two directions. In their model fragment mass and energy distributions are determined by the branching ratios at the bifurcation points and by random neck rupture as hydrodynamical Rayleigh instabilities of the scission configurations at the end of each fission path.

The increased intensity of the neutron source of the European neutron time-of-flight spectrometer of the Central Bureau for Nuclear Measurements at Geel and the development of the double Frisch-gridded ionization chamber /4,5/ have now allowed the measurement of complete fragment mass and energy distributions in resolved resonances of the reaction $^{235}U(n,f)$ /6,7/.

2. Results and discussion

The results of the present measurements are fission fragment yields, $Y(M, TKE, \cos\delta, E_n)$, as function of the fragment mass M, the total fragment kinetic energy TKE, the cosine of the angle δ between the incident neutron beam direction and the direction of propagation of the fission fragment, and the incident neutron energy E_n. This multi-parametric measurement covers the neutron energy range from 0.006 eV to 0.5 MeV. The angular dependence of the fragment emission is important only at higher incident neutron energies. Therefore, the $\cos\delta$ -dependence is not considered in the data evaluation for the resolved resonance region from 0.006 eV to about 140 eV, where mass-, and average TKE-distributions were evaluated for 54 isolated resonances, resonance clusters or energy bins /6,7/. The energy intervals chosen for the evaluation of the present experiment are the same as in the ν-experiment of Howe et al./8/.

The fragment yield for each isolated resonance or incident neutron energy bin Y(M,TKE) can be represented by the integrated mass distribution Y(M), the average total kinetic energy as function of mass split TKE(M),

Present addresses:
* Carl Schenck A.G., Darmstadt, Germany
** Danish Space Research Institute, DK-2800 Lyngby

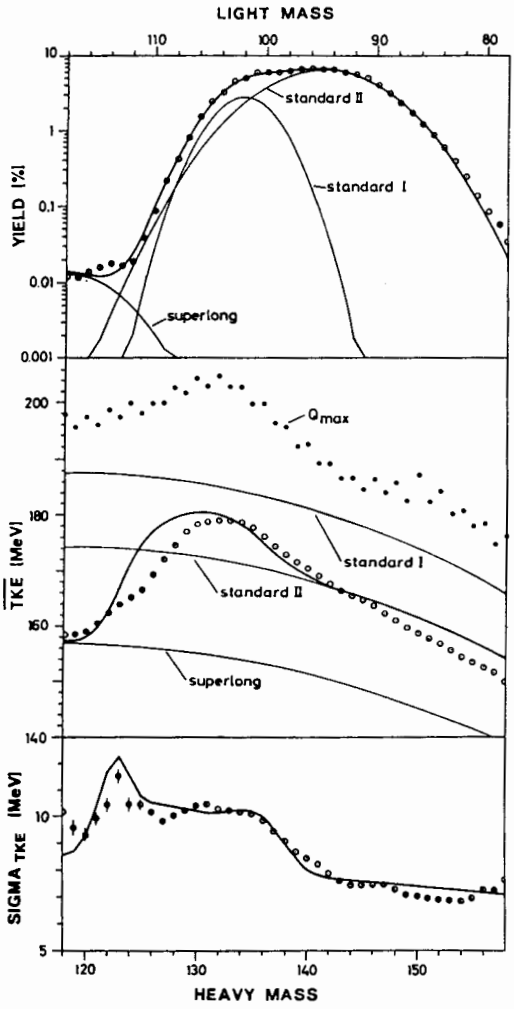

Fig. 1 Fission fragment distributions of $^{235}U(n,f)$ for thermal neutrons are plotted versus the mass split. Fig. 1 is taken from Knitter et al./9/.

sigma$_{TKE}$(M) and higher moments of the TKE(M)-distributions.

2.1. Results and discussion for thermal neutrons.

For the thermal neutron induced fission of $^{235}U(n,f)$ the experimental fission fragment mass distribution, the average total kinetic energy TKE as function of mass, and the square root of the variance of the TKE distribution as function of mass are shown in fig. 1.

Recently, Brosa et al./2,3/ performed Strutinski-type calculations for several nuclei covering the mass range from ^{227}Ac to ^{258}Fm where the potential energy of the compound system was calculated also for large deformations up to the scission point. These calculations indicate the presence of several fission modes, paths or exit channels, whose accessibilities are different for different fissioning nuclei. For $^{235}U(n,f)$ they predict three fission exit channels, which result in three different scission shapes of the compound system. This picture permitted Knitter et al. /9/ to develop a simple mathematical description for the fission fragment yield as function of mass and total kinetic energy Y(M,TKE). In this description the total fission fragment mass distribution is a superposition of three Gaussian frequency distributions, one for each fission exit channel.

The mass distribution of each fission channel is determined by its relative population W_i, and by the average mass M_i and width σ_{M_i} of the Gaussian mass distribution. The three Gaussian distributions describing the superlong, standard I and standard II fission mode mass distributions are plotted in the upper part of fig. 1 as full lines. The full line through the experimental points shows the sum of the three Gaussians. The curves were obtained by fitting the experimental mass distribution data for thermal neutron induced fission of ^{235}U.

The values for the average masses M_i and variances $\sigma^2_{M_i}$ of the mass distributions for the three fission modes are in agreement with the values from theory /9/. In the above model a different but specific scission shape belongs to each fission mode which is characterized e.g. by the distance D_i between the two charge centres and their mass and charge ratios. The total kinetic energy of the fragments is calculated as the

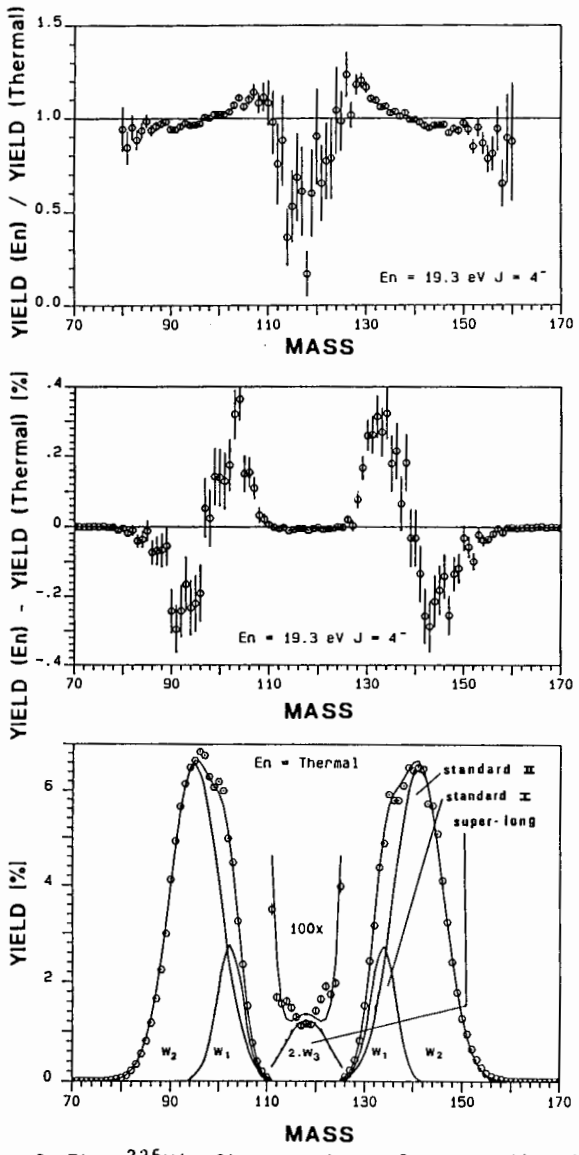

Fig. 2 The $^{235}U(n,f)$ experimental mass distribution for thermal neutrons and the partial and global mass distributions obtained from the fit are plotted as full lines versus the mass. In the middle and upper part the yield difference and ratio of the mass distribution measured in the 19.3 eV resonance and for thermal neutrons are plotted, respectively.

Coulomb repulsion energy neglecting other smaller terms. The variances of the TKE-distributions are obtained assuming a Gaussian frequency distribution for the charge distance D around the average D_i with a width σ_{D_i}. This representation of the fission fragment yield as function of mass and TKE was used to fit the experimental data for the average total kinetic energy as function of mass TKE(M) and the square root of the variance of the TKE-distribution $\mathrm{sigma}_{TKE}(M)$. The parameters D_i and σ_{D_i} obtained by the fit are also in agreement with theory /9,10/. In the middle part of fig. 1 there are three thinner lines representing the average TKE as function of mass for each fission exit channel. The thicker line, following the experimental points within 5%, is the average total kinetic energy composed of those from the three exit channels. This model can explain for the first time the drop of the average TKE(M) towards mass symmetry.

The large variance values of the TKE distributions are not understood by any previous fission model /1/. As shown in the lower part of fig. 1 the present description of a three exit channel model can cope also with the sigma distribution. Below mass 140 the superposition of the exit channels is responsible for the higher values of $\sigma_{TKE}(M)$, since the exit channels have different average energies.

2.2. Results and discussion of the resonance region.

Mass and TKE distributions are evaluated for the isolated resonances and resonance clusters. As an example for many resonances fig. 2 shows in three parts, the mass distribution for thermal neutron induced fission and the difference and the ratio of the mass distribution with respect to the thermal distribution measured for the 19.3 eV resonance . The yield difference brings into evidence an increase of the population of the standard I channel and a decrease of the standard II channel with respect to the thermal distribution. The ratio of both spectra in the upper part of fig. 2 shows a decrease of the symmetric fission yield by about a factor of two compared with the yield for thermal neutrons.

The fluctuations in the partial mass distribution yields W_i observed from resonance to resonance represented e.g. by $(W_1/W_2(E_n))$ /$(W_1/W_2$ (thermal)) must be correlated with the total kinetic energy averaged over all fragments, $\langle TKE\rangle_{E_n}$, and also with the average reaction Q-value, $\langle Q\rangle$, since both are functions of the mass split. These correlations are shown in fig. 3.

Fluctuations in $\langle TKE\rangle_{E_n}$ up to ~450 keV are observed within a change in neutron energy by only a few eV. In fig. 4 the $\langle TKE\rangle_{E_n}$- values of the isolated resonances below 40 eV neutron energy are selected with respect to the resonance spins 3^- and 4^-. However no spin dependence can be deduced from this observation (6,7).

The A_2-coefficient of fission fragment angular distributions measured in alignment experiments as e.g. by Pattenden et al. (11) is given in the case of $^{235}U(n,f)$ by

$$A_2 = 2.917 \left\{ \frac{3K^2}{J(J+1)} - 1 \right\} \qquad (1)$$

where K is the orientation quantum number of the spin J with respect to the symmetry axis of the

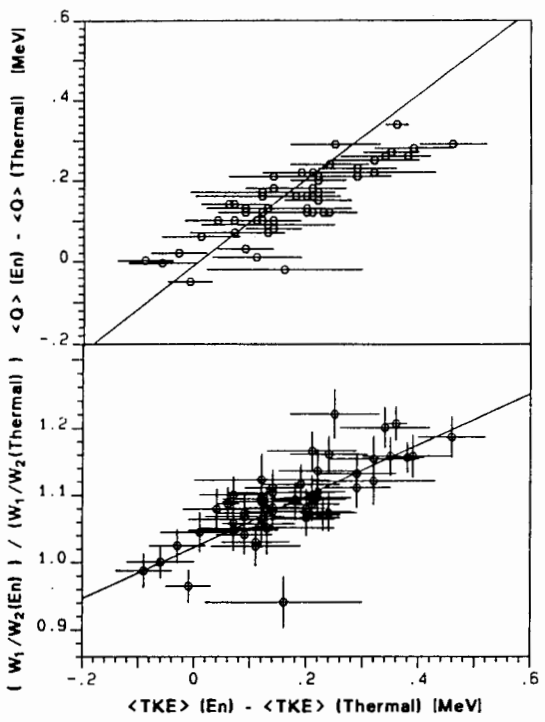

Fig. 3 Correlation diagram for the relative (standard I)/(standard II) fission mode populations and the relative <Q>-values versus the relative <TKE>-values are shown in the lower and upper part respectively.

compound system. Equation (1) leads to discrete values for fixed K and J. The correlation diagram between the experimental A_2-values of Pattenden et al. and the valley to peak ratios of the mass distributions of the present work and those of Cowan et al./12/ are shown in fig. 5. A correlation coefficient of $r = (0.81 \pm 0.05)$ is obtained. A separation with respect to the two spin states gives a similar correlation in both cases.

Since no accumulation of the experimental A_2-values near the discrete values for fixed J according to equation (1) is found, K-mixing must be present in the excited compound states of fixed J. This was concluded also by Keyworth et al./13/ from the frequency distribution of the A_2-coefficients for resonances with the same J.

3. Conclusions

The gross structure of the mass distribution of the thermal neutron induced fission of ^{235}U is

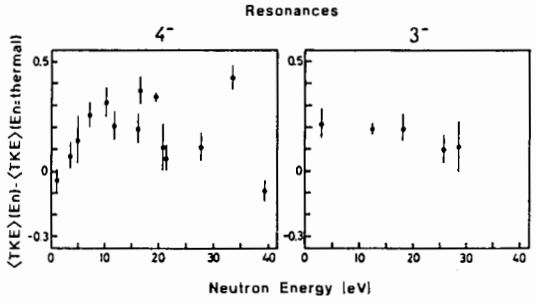

Fig. 4 Relative <TKE>-values for 4^- and 3^- resonances.

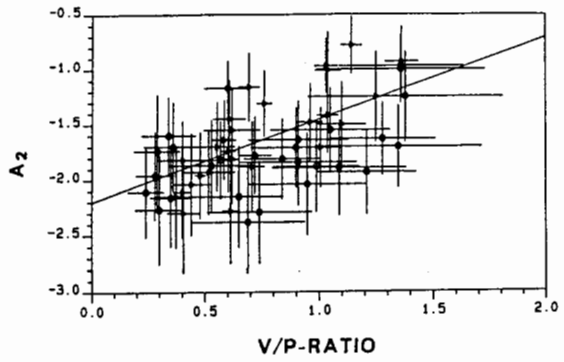

Fig. 5 Correlation diagramme for the A_2-angular distribution coefficients and the V/P-ratios.

well described by the sum of three Gauss functions which can be interpreted as individual contributions of the three fission channels as proposed in the Brosa-Grossmann-Müller model /2/. The fitted curve through the experimental average total kinetic energies as shown in fig. 1 deviates nowhere by more than 5 % from the experiment. However from the physics point of view it is more important that the shape of the curve and the large drop for symmetric fission are understood in the frame of the above model. The presence of the three independent channels is also reflected in the curve for sigma. Agreement between experiment and theory is found for the model parameters M_i, σ_{M_i}, D_i and σ_{D_i} /9,10/. The experimental increase of symmetric fission in the MeV range /7,14/ can be understood by an increased transmission through the high barrier found in the superlong fission path.

The asymmetric mass distribution peak is composed of the standard I and standard II channel mass distributions. Since the branching point for both channels is at or slightly after the second saddle the model predicts 50 % for W_1 and W_2, whereas the experiment gave $W_1 \approx 20$ % and $W_2 \approx 80$ %. However, dynamical effects might explain this difference The branching ratios show fluctuations from resonance to resonance, and no clear dependence on J was detected. The potential energy surface near the branching point is flat and the deforming nucleus needs no additional energy to decide between one or the other path. The transition time from saddle to scission is about 10^{-21} s. This corresponds to an energy uncertainty of 0.5 MeV. It means that the fluctuations in the branching ratio cannot arise from different potential forms of the transition states at the branching, since their distances are smaller than their widths. The transition time at the saddle is of the order of 10^{-20} s and the energy uncertainty of the saddle point states is then of the order of $\approx$10 keV. Therefore, the branching behaviour must already be fixed before the transition states at the saddle are reached. The collective transition states of the Bohr-Wheeler model with fixed quantum numbers J,K and π cannot describe the true behaviour of the multi-particle wave function of the deformed compound nucleus. The branching ratio fluctuations might be an indication that the collective saddle point transition states are only appproximations.

Each of the Brosa exit channels must possess one or more accessible nuclear states. If the matrix elements between the compound state and these states are small and Gaussian distributed, the partial fission widths $\Gamma_{f,i}$ will be χ^2_n distributed, like it is normally the case for Γ_f. Therefore the branching ratios

$$R_i = \frac{\Gamma_{f,i}}{\sum_i \Gamma_{f,i}} \quad with \quad \Gamma_f = \sum_i \Gamma_{f,i}$$

will fluctuate. The number of degrees of freedom n per exit channel should then reduce compared to the number of degrees of freedom of the total fission width Γ_f.

REFERENCES

1) Yu. T. Oganessian and Yu. A. Lazarev
Treatise on Heavy-Ion Science, Vol. 4, Extreme Nuclear States, Editor : D.A. Bromley, Plenum Press (N.Y. and London), page 1-255 (1984).

2) U. Brosa, S. Grossmann, and A. Müller
Z. Naturforsch. 41a, 1341 (1986)

3) U. Brosa, S. Grossmann, and A. Müller
Proc. of the XVIth Int. Symp. on Nuclear Physics Dresden, Germany, Nov. 1986.

4) H.-H. Knitter, and C. Budtz-Jørgensen
Proc. Intern. Conf. on Nuclear Cross Sections and Technology, Knoxville, U.S.A.
NBS-Special Publication 594, 947 (1980)

5) C. Budtz-Jørgensen, H.-H. Knitter, Ch. Straede, F.J. Hambsch, and R. Vogt
Nucl. Instr. Meth. A285, 209 (1987)

6) F.-J. Hambsch, PhD-Thesis, CBNM-Geel and TH Darmstadt (1987)

7) H.-H. Knitter, F.-J. Hambsch, C. Budtz-Jørgensen, and J. P. Theobald
Proc. of Intern. Conf. on Neutron Physics, 21st-25th Sept. 1987, Kiew USSR

8) R.E. Howe, T.W. Phillips, and C.D. Bowman
Phys. Rev. C13, 195 (1976)

9) H.-H. Knitter, F.-J. Hambsch, C. Budtz-Jørgensen, and J. P. Theobald
Z. Naturforsch. 42a, 786 (1987)

10) S. Grossmann, U. Brosa, and A. Müller
to appear in Nucl. Phys. A

11) N.J. Pattenden, and H.H. Postma
Nucl. Phys. A167, 225 (1971)

12) G.A. Cowan, B.P. Bayhourst, E.J. Prestwood, J.S. Gilmore, and G.W. Knobeloch,
Phys. Rev. C2, 615 (1970)

13) G.A. Keyworth, C.E. Olsen, J.D. Moses, J.W.T.-Dabbs, and N.W. Hill
Intern. Conf. on Cross Section and Technology, Washington D.C.,U.S.A.
N.B.S. Special Publication 425, 576 (1975)

14) Ch. Straede, C. Budtz-Jørgensen and H.-H. Knitter
Nucl. Phys. A462, 85 (1987)